EVALUATION OF STRUCTURAL PROPERTIES OF CYLINDRICAL PACKED BEDS USING NUMERICAL SIMULATIONS AND THOMOGRAPHIC EXPERIMENTS

W. I. Salvat[1], N. J. Mariani[1,2], M. A. Campesi[1,2], G. F. Barreto[1,2], O. M. Martínez[1,2♣]

[1]PROIRQ, Área departamental de Ingeniería Química, Facultad de Ingeniería

Universidad Nacional de La Plata, La Plata, Argentina

[2] Centro de Investigación y Desarrollo en Ciencias Aplicadas "Dr. J. J. Ronco" (CINDECA)

CONICET- Universidad Nacional de La Plata

Calle 47 No. 257, CP B1900AJK, La Plata, Argentina

(♣) Osvaldo M. Martínez
Centro de Investigación y Desarrollo en Ciencias Aplicadas "Dr. J. J. Ronco" (CINDECA)
CONICET- Universidad Nacional de La Plata
Calle 47 No. 257, CP B1900AJK, La Plata, Argentina
Phone number: #54-221-4210711
Fax number: #54-221-4210711 (Int. 125)
email: ommartin@ing.unlp.edu.ar

ABSTRACT

This contribution is focused on the analysis of the structure of packed beds of spherical particles at relatively low aspect ratios (*i.e.*, particle to tube diameter ratio) as those arising in multitubular fixed bed reactors. On one hand, the computed tomography (CT) technique is employed to evaluate the position of each particle in the packing and from this information local properties such as particle center distribution and radial porosity profile were obtained. On the other hand, results from a previously developed algorithm to simulate packings were compared with those from our CT data and from literature sources. The agreement was very satisfactory.

Keywords: packing structure, packed-bed generation, computed tomography, radial porosity profile

INTRODUCTION

Cylindrical packed beds are widely used in almost all chemical process industries. Examples of paramount importance are catalytic fixed bed reactors with either single or two-phase flow. The model employed to simulate the reactor determines the degree of information required about the packed bed structure (Dixon et al., 2006; Castillo-Araiza et al., 2007). For the nowadays increasing use of the Computational Fluid Dynamics (CFD) it becomes necessary to know the positions of all particles in the bed. In addition, aiming to formulate heterogeneous discrete models for catalytic reactors it should be feasible to estimate the spatial distribution of the solid phase.

Many experimental studies on packing structure have been made during the last decades from different points of view. Destructive and non-destructive techniques have been used to obtain packing information of different types. For the most part, the former investigations have been focused on the evaluation of porosity and empirical expressions have been proposed to predict overall porosities and radial porosity profiles (Mariani et al., 1998, de Klerk, 2003). However, a much complete description of particle packing is obtained by evaluating the location of particle centers in the bed. This can be accomplished by employing several non-destructive techniques: X-ray radiography (Mueller, 1991), X-ray computed tomography (Toye et al., 1998; Irazoqui et al., 2004; Suzuki et al., 2008), gamma-ray computed tomography (Wang et al., 2001), magnetic resonance imaging (Ren et al., 2005), among others. Indeed, packing properties arise as a consequence of the location of the particles in the bed (Mariani et al., 2002). Hence, it is clear that the knowledge of the location of the particles is the more basic information about the packing structure. Overall bed porosity, radial and axial porosity profiles, contact-point distribution, particle center distribution and external surface area profiles can be readily evaluated from the knowledge of particle location (Mariani et al., 2001).

A convenient alternative to conduct experimental measurements for particle locations in the bed arises from the development of computational tools to simulate particle packing. A classification of 3D algorithms to generate packed bed structure can be made by distinguishing between soft and hard sphere approaches, depending on the allowance of overlapping between spheres or not. A discussion of the several approaches to formulate 3D algorithms has been undertaken by Salvat et al. (2005).

In a previous paper (Salvat et al., 2005) we have presented an algorithm to simulate the structure of packed beds of spherical particles of uniform size in cylindrical containers, which is based on the soft spheres approach. The algorithm renders the position of each sphere in the container. Experimental data of overall bed porosities from different sources were employed to successfully validate the results obtained by simulation (Salvat et al., 2005).

The main purpose of this contribution is to present results for local packed-bed properties obtained by simulation and compare them with experimental data from different sources, including X-ray Computed Tomography (CT) experiments for selected aspect ratios (*i.e.*, tube to particle diameter ratio) first reported in this paper. Special attention is given to the low range of aspect ratios, typical of fixed bed reactors exchanging heat through the wall, where experimental data are scarce. Simulated and experimental results are analysed by emphasizing the relation between particle center distribution and radial porosity profiles.

MODEL AND ALGORITHM FOR SIMULATING BED PACKING

When loading a cylindrical container with solid particles, an equilibrium condition is reached just when all forces acting on every particle are balanced. They are gravitational,

friction and contact forces. Also, there are two physical restrictions to sphere accommodation: vessel and bottom walls.

It has been experimentally demonstrated that while a vessel is being filling with particles friction forces inhibit their close accommodation. From a practical point of view, however, particles in an actual packed bed become more tightly accommodated by the effect of vibration (Nowak et al., 1997) or after some period on operation. As the algorithm to be described next simulates the accommodation of particles from a certain initial condition, friction forces between particles and between particles and the vessel wall have been ignored, expecting in this way that the results for the final resting position of the particles closely resembles a real packed bed on operation.

To account for the effect of contact forces, a certain degree of interpenetration between the spheres is allowed. The repulsion force generated from interpenetration is assumed to be proportional to the overlapping magnitude, as in elasticity theory. In an early stage of the procedure, the intensity of the repulsive force is kept relatively low, while in the final stage the intensity is increased so as to produce a very tiny overlap. The effect gained from this strategy is the achievement of more compact beds, closer to those found in practice.

The lateral wall of the container will also be considered as a deformable body. The force exerted by the lateral wall on a contacting sphere is radially directed towards the container axis.

The behavior of the base of the bed should also be defined. Although the base might be considered as being deformable too, it has been checked that this feature brings no significant consequence for the results. Therefore, a rigid base exerting an action to balance the axial force on each particle resting on is assumed.

Summarizing, the following features are considered in formulating the algorithm to generate packed beds in cylindrical containers: a) the spheres are mono-sized; b)

gravitational field is accounting for; c) the friction forces are neglected; d) the spheres as well as the lateral wall are deformable; e) the base of the container is rigid; f) the contact forces between spheres and between spheres and the wall are evaluated on the basis of elasticity theory.

The net force $\vec{F}_{i,\,n}$ acting on the i-th sphere can be expressed as,

$$\vec{F}_{i,\,n} = \vec{F}_{i,\,Lw} + \vec{F}_{i,\,Bw} + \vec{W} + \sum_{j} \vec{F}_{ij,C} \tag{1}$$

where:

$\vec{F}_{i,\,Lw}$: force exerted by the lateral wall on the i-th sphere

$\vec{W}$: sphere weight

$\vec{F}_{ij,C}$: contact force exerted by the j-th sphere on the i-th sphere

$\vec{F}_{i,\,Bw}$: force exerted by the container's bottom on the i-th sphere

All forces acting on every sphere pass through the center of mass, therefore it is not necessary to set out torque balances.

The formulation for every force is:

$$\vec{F}_{i,Lw} = -k\ R(\delta_{iw})\,\hat{r} \quad (2a); \qquad \vec{F}_{ij,C} = -k\ R(\delta_{ij})\,\hat{d}_{ij} \quad (2b); \qquad \vec{W} = -M\,g\,\hat{z} \quad (2c)$$

where

$$\text{R}(\xi)\text{: Ramp function} = \begin{cases} 0, & \text{if} \quad \xi \le 0 \\ \xi, & \text{if} \quad \xi > 0 \end{cases}$$

δ_{ij}: overlapping between i-th sphere and j-th sphere $= D_p - \left\| \vec{x}_i - \vec{x}_j \right\|_2$

δ_{iw}: overlapping between i-th sphere and the lateral wall $= (r_i + D_p/2) - R_t$

The forces $\vec{F}_{i,\,Bw}$ are not formulated because it is supposed that their values are just enough to make zero the axial component of $\vec{F}_{i,\,n}$ of those spheres contacting the container

bottom. It is worth remarking that $\vec{F}_{i,\,Lw}$ and $\vec{F}_{ij,C}$ are repulsive in nature and they become nil when there is no overlapping (Eqs. 2a,b). For the sake of simplicity the constant k is assumed to be the same for both, $\vec{F}_{i,\,Lw}$ and $\vec{F}_{ij,C}$.

Once the aspect ratio $a=2R_t/D_p$ and the number of particles N_p are defined, the purpose of the algorithm described next is to define a set of positions for all particles that will render $\vec{F}_{i,\,n}=\vec{0}$ (in an approximate sense) for i=1,…, N_p.

Algorithm

The algorithm can be described considering four stages: generation, initial, intermediate and final stages. The generation stage is needed to define an initial distribution of particles, while the other three stages are characterized by a specific effect on the packing structure (expansion, compaction, force balancing). Even when the division into stages is somewhat arbitrary, it arises as a result of tuning the algorithm to attain robustness and better convergence speed. The following quantities should be monitored to identify the transition between each stage: packing mass center (MC), maximum overlapping between particles ($\delta_{ij,max}$) and maximum overlapping between particles and the wall ($\delta_{iw,max}$).

Except in the generation stage, the displacement of particles is guided by the need to reduce the net force ($\vec{F}_{i,n}$) acting on every sphere. From the values $\vec{x}_i^{\,m}$ and $\vec{F}_{i,n}^{\,m}$ at iteration m, the new position $\vec{x}_i^{\,m+1}$ of the i-th sphere is calculated as:

$$\vec{x}_i^{\,m+1}=\vec{x}_i^{\,m}+U^m\,\vec{F}_{i,n}^{\,m} \tag{3}$$

where U^m is the step-length chosen at iteration m. Substituting $\vec{F}_{i,n}$ according to Eqs. (1) and (2)

$$\vec{x}_i^{\,m+1}=\vec{x}_i^{\,m}-C_k^m\left[R(\delta_{iw}^m)\,\hat{r}+\sum\nolimits_j R(\delta_{ij}^m)\,\hat{d}_{ij}\right]-C_g^m D_p\hat{z} \tag{4}$$

$$C_k^m = k^m U^m \qquad (5a); \qquad C_g^m = M\, g\, U^m D_p^{-1} \qquad (5b)$$

C_k^m and C_g^m are the elasticity and gravity parameters at iteration m. As the elasticity parameter will have to be changed in the course of the calculations, it is also written generically as dependent on the iteration level, k^m.

Further details about the algorithm operation were described elsewhere (Salvat et al., 2005).

MATERIALS AND EXPERIMENTAL METHOD

Acrylic tubes were packed with mono-sized spherical polypropylene particles. As a first step, particles were carefully selected to warrant a uniform size and the tube was randomly filled. With the aim of achieving a reproducible procedure to obtain compact packings (often called *dense random packing*) a commercial shaker was used. Shaking was applied until the bed height remains unchanged. Once shaking was stopped the packing was conveniently fixed to avoid further displacement of the particles.

Experimental results from two aspect ratios (a=4.29 and a=5.04) will be presented and analyzed in this contribution. For both packed beds the bed height to particle diameter ratio was set to be greater than 50 to assure that "ends effects" are negligible (Zou and Yu, 1995).

X-ray computed tomography (CT) studies were carried out in a PICKER PQ5000 helical tomograph with a BOXELQ workstation, set up in a medical center (*Centro de Imágenes Médicas* – CIMED) at La Plata, Argentina.

In order to illustrate the results of the procedure to obtain images, Figure 1 shows eight consecutive cuts for a packing having an aspect ratio a=4.29. A spherical particle is viewed as a white circular contour with a diameter depending on the distance between the cut and the parallel plane containing the particle center. At least two cuts intersecting the same

sphere are needed to determine the position of its center; hence, the space between cuts should avoid the chance of missing a particle. Then, the space was set in about a third of a particle diameter. It is worth mentioning that cuts near a sphere pole generally lead to blurred contours, as can be appreciated for the pointed particle in Figure 1 (a). On the contrary, for cuts (b) and (c) in Figure 1, the same particle was intersected relatively far from its poles and the resulting contour becomes very well defined. Another important aspect to facilitate the image processing is to reduce as much as possible the thickness of the tomographic cut (known as *slice*). The least thickness allowed by the apparatus (1 mm) was adopted for all experiments. Besides, spheres with a considerable larger diameter than the slice thickness were employed (D_p=0.02504 m for a=4.29 and D_p=0.01905 m for a=5.04).

The images obtained by tomography were processed by means of a code written in Visual Basic. For each contour, a dummy circle was drawn to exactly match it. The procedure repeated for at least two cuts showing the same sphere readily allows evaluating the position of the sphere center.

From the above summarized image processing, the position (angular, radial and axial coordinates) of each sphere center in the packing could be calculated.

RESULTS AND DISCUSSION

From the position of all sphere centers in the packing it is possible to evaluate all the packing properties at local or global scale (Mariani et al., 2001). Due to the fundamental character of particle center distribution, it is convenient first to analyze this property from experimental and simulated points of view.

Experimental and simulated radial distribution of particle centers

Figure 2.a shows the radial distribution of particle centers experimentally obtained by CT for a=5.04. A highly ordered first layer of particles adjacent to the tube wall (from a distance of about one particle radius) can be clearly appreciated. Besides, a more diffuse second layer can be identified toward the inside of the bed. A relatively dispersed number of centers are observed in the region closer to the tube axis. In Figure 2.b the simulated radial distribution of particle centers for the same aspect ratio (a=5.04) is presented. It can be appreciated that both, experimental and simulated, distributions show the same pattern. Some visual differences between Figures 2.a and 2.b arise because the number of particles employed in the simulation is larger than in the CT experiments. Thus, particles located in the region around the tube axis tend to gather in an even more diffuse third layer, as can be seen from the simulation in Figure 2.b.

Aiming to quantitatively compare experimental and simulated radial distributions of particle centers, the cumulative fraction of particle centers (CPC) (set to zero at the tube axis) is presented in Figure 3 as a function of dimensionless radial coordinate $\rho = r/D_p$ (*e.g.*, at the tube wall $\rho = 2.52$, for a=5.04).

It is clear from Figure 3 that the curves for experimental (a) and simulated (b) distributions match very well, even when the number of particles used in both cases is different. Sharp slopes at certain radial positions indicate a high concentration of particle centers. Approximately 60 % of the particles are located in the layer against the wall; 30% in the second layer, at a distance slightly lower than one and a half particle diameters from the tube wall. The remaining 10% are more or less dispersed in the region of the center of the tube ($\rho<1$).

From the curve (c) of Figure 3, it can be appreciated that a slight increase in aspect ratio (from 5.04 to 5.60) leads to the building of a fairly neat third particle layer close to

the tube axis, as revealed by the steep increase in the cumulative fraction of particle centers in the range $0.5<\rho<0.7$ (2.1-2.3 particle diameters from the tube wall).

From the comparison between curves (b) and (c) of Figure 3, it can be concluded that more particles stay in the region close to the bed axis for a=5.04 than for a=5.60. This fact leads in turn to lower local porosities for a=5.04. This observation will be further discussed in the next section.

The radial density distribution of particle centers (RPC) is presented in Figure 4 for a=5.04 (simulated results). For the sake of convenience, the sharp peak corresponding to the first layer of particles at $\rho\approx2.02$ was omitted. The distributions correspond to two bed slices of about 300 particles at different axial positions of the same packing. Ends effects are negligible in both slices. Even when the curves are very similar, slight differences in numerical values arise. These differences will be reflected in the values estimated for the rest of the packing properties (*e.g.*, radial porosity).

Radial porosity profile

It is worth recalling that all the local packing properties, including the radial porosity profile, can be obtained from the radial distribution of particle centers, by following the approach proposed by Mariani et al. (2001). Basically, to evaluate the local porosity at a certain radial position the areas of the intersection of the spheres in the bed with the surface of an imaginary cylinder coaxial with the bed at that radius should be computed.

The comparison between experimental and simulated radial porosity profiles for two aspect ratios, a=5.04 and a=4.29 is presented in Figures 5 and 6. The profiles are plotted as a function of the dimensionless distance from the vessel wall, $y= (R_t-r)/D_p$ and correspond to average values along the whole bed height.

Both porosity profiles, experimental and simulated, are almost indistinguishable from y=0 to y≈1 (approximately the first maximum). In addition, the position and the values of the extrema (maximum and minima) present a remarkable agreement.

The more noticeable, but still moderate, differences in Figures 5 and 6 can be observed towards the tube axis. Concerning these differences, some comments are worthy. First, it should be pointed out that the differences can be attributed to some randomness of the packing in this region. If the radial porosity is evaluated in different bed slices along the bed axis, instead of on the whole height, fluctuating values arise. For example, taking slices of 5 cm height, the values of local porosity at y=2 in the simulated packing with a=4.29 range from 0.636 to 0.893. This variation is caused by the dispersion of particles centers in the second layer of the different slices.

Although it can be concluded that local porosity in the region close to the tube axis can not be predicted without a certain level of uncertainty, it is also clear that in this region the local porosity are definitely lower at a=5.04 (Fig. 5) than at a=4.29 (Fig. 6). This is due to the fact that the aspect ratio a=5.04 allows the accommodation of a significant number of particles centered close to the tube axis (see Fig. 3, curves a and b), while a=4.29 does not (see the images in Figure 1).

A similar situation as for a=4.29 occurs for a =5.60 (Figure 3, curve c).

The radial porosity profile for a=5.60 obtained by simulations is compared in Fig. 7 with experimental data from Benenati and Brosilow (1962). It is worth noting that the three minima arise as a consequence of the existence of three ordered layers of particles. A very good agreement between both profiles is evident from Fig. 7.

To further test the algorithm to simulate packings, the experimental porosity profile from Giese et al. (1997) at a higher aspect ratio of a = 9.30 is compared in Figure 8 with the simulated profile. The latter closely follows the experimental data. For this aspect ratio

(a=9.30) the typical damped oscillatory behavior of the radial porosity profile can be clearly observed.

It is important to mention that other comparisons between simulations and experimental data from different sources with aspect ratios ranging from 4 to ∞ were carried out. In general, the agreement was highly satisfactory.

CONCLUSIONS

With the aim of analyzing the structure of packed beds of mono-sized spherical particles in cylindrical containers two tools have been employed: experimental data from X-ray computer tomography (CT) and simulated results obtained by using a numerical algorithm previously proposed. In both cases, all local and global properties of the bed can be calculated from the known position of the particles in the bed.

The radial distribution of particle centers and porosity profiles evaluated from the CT data at relatively low aspect ratios were satisfactorily compared with the results predicted by the algorithm.

In addition, simulated radial porosity profiles were compared with experimental data from different literature sources with the purpose to further test the algorithm predictive capabilities. In all cases, results from the simulation agree very well with the experimental profiles and a remarkable matching of the position and the value of the extrema was also evident.

From the above summarized results it can be concluded that the developed algorithm is an adequate tool to predict local packed bed properties.

Acknowledgements

The authors wish to thank the financial support of the following Argentine Institutions: CONICET (PIP 6414), ANPCyT- SECyT (PICT N# 14/38336), UNLP (PID N# 11/I100). The authors are also grateful to *Fundación CIMED* (La Plata, Argentina) for providing the access to the tomography equipment. N. J. Mariani, O. M. Martínez and G. F. Barreto are research members of the CONICET; M.A.Campesi is a fellow of CONICET.

NOMENCLATURE

a: aspect ratio, $= 2R_t/D_p$

C_k^m: elasticity parameter at the m-th iteration , $= k^m U^m$

C_g^m: gravity parameter at the m-th iteration, $= M\ g\ U^m\ D_p^{-1}$

D_p: sphere diameter [m]

$\hat{d}_{ij}$: unit vector defined from the center of the i-th sphere to the center of the j-th sphere

$\vec{F}_{i,\,Bw}$: force exerted by the container's bottom on the i-th sphere [N]

$\vec{F}_{ij,C}$: contact force exerted by the j-th sphere on the i-th sphere [N]

$\vec{F}_{i,\,Lw}$: force exerted by the lateral wall on the i-th sphere [N]

$\vec{F}_{i,\,n}$: net force acting on the i-th sphere [N]

g: acceleration of gravity [m s^{-2}]

k: elasticity coefficient [N m^{-1}]

L: packing height [m]

M: sphere mass [kg]

N_p: total number of particles in the packing

R_t: container radius [m]

r_i: radial coordinate of i-th sphere measured from the container axis [m]

$\hat{r}$: radial unit vector

U^m: step-length at the m-th iteration [m N^{-1}]

$\vec{W}$: gravitational force on a sphere [N]

x: dimensionless radial coordinate measured from the container wall, $=(R_t-\rho)/D_p$

$\vec{x}_i^m$: position vector of the i-th sphere at the m-th iteration [m]

y: dimensionless distance from the vessel wall, = $(R_t\text{-}r)/D_p$.

z: axial coordinate measured from the bottom of the bed [m]

$\hat{z}$: axial unit vector (upwardly oriented)

Greek letters & Special symbols

δ_{ij}: overlapping between i-th sphere and j-th sphere,= $D_p - \left\|\vec{x}_i - \vec{x}_j\right\|_2$ [m]

$\delta_{ij,max}$: maximum value out of all δ_{ij} [m]

δ_{iw}: overlapping between i-th sphere and the lateral wall, = $(r_i + D_p/2) - R_t$ [m]

$\delta_{iw,max}$: maximum value out of all δ_{iw} [m]

ρ: dimensionless radial coordinate $=\rho/D_p$

$\|\bullet\|_2$: Euclidean norm

REFERENCES

Dixon, A.G., M. Nijemeisland, E.H. Stitt, Packed tubular reactor modeling and catalyst design using computational fluid dynamics, Advances in Chemical Engineering 31 (2006) 307-389.

Castillo-Araiza, C.O., H. Jiménez-Islas, F. Lopez-Isunza, Heat transfer studies in packed-bed catalytic reactors of low tube/particle diameter ratio, Ind. Eng. Chem. Res. 46 (2007) 7426-7435.

Mariani, N.J., G.D. Mazza, O.M. Martínez, G.F. Barreto, The distribution of particles in cylindrical packed beds, Trends in Heat, Mass and Momentum Transfer 4 (1998) 95-114

de Klerk, A., Voidage variation in packed beds at small column to particle diameter ratio, A.I.Ch.E. J. 49 (2003) 2022-2029.

Mariani, N.J., W.I. Salvat, O.M. Martínez, G.F. Barreto, Packed bed structure: evaluation of radial particle distribution, The Can. J. Chem. Eng. 80 (2002) 186-193

Mariani, N.J., O.M. Martínez, G.F. Barreto, Computing radial packing properties from the distribution of particle centers, Chem. Eng. Sci. 56 (2001) 5693-5707.

Salvat, W.I., N.J. Mariani, G.F. Barreto, O.M. Martínez, An algorithm to simulate packing structure in cylindrical containers, Catal. Today 107-108 (2005) 513-519.

Nowak, E., J. Knight, M. Povinelly, H. Jaeger, S.Nagel, Reversibility and irreversibility in the packing of vibrated granular material, Powder Technol. 94 (1997) 79-83.

Zou, R.P., A.B.Yu, The packing of spheres in a cylindrical container: the thickness effect. Chem. Eng. Sci. 50 (1995) 1504-1507.

Benenati R., C.B. Brosilow, Void fraction distribution in bed of spheres, A.I.Ch.E.J. 8 (1962) 359-361.

Giese, M., K. Rottschäfer, D. Vortmeyer, Measured and modelled superficial flow profiles in packed beds with liquid flow, A.I.Ch.E. J. 44 (1998) 484-490.

J. Götz, K. Zick, C. Heinen, T. König, Visualisation of flow processes in packed beds with NMR imaging: determination of the local porosity, velocity vector and local dispersion coefficients, Chemical Engineering and Processing 41 (2002) 611–629.

M. Suzuki, T. Shinmura, K. Iimura, M. Hirota, Study of thec Wall Effect on Particle Packing Structure Using X-ray Micro Computed Tomography, Advanced Powder Technology 19 (2008) 183–195.

H. A. Irazoqui, M. A. Isla, R. J. Brandi, A. E. Cassano, Packed-Bed Photocatalytic Reactors. A Packing Structure Model and Its Experimental Validation with Computerized Tomography, Ind. Eng. Chem. Res. 43 (2004) 1430-1442.

D. Toye, P. Marchot, M. Crine, A. M. Pelsser, G. L'Homme, Local measurements of void fraction and liquid holdup in packed columns using X-ray computed tomography, Chem. Eng. & Process., 37 (1998) 511–520

Mueller, G.E., Prediction of Radial Porosity Distributions in Randomly Packed Fixed Beds of Uniformly Sized Spheres in Cylindrical Containers, Chem. Eng. Sci., 46-2 (1991) 706-708.

Z. Wang, A. Afacan, K. Nandakumar, K. T. Chuang, Porosity distribution in random packed columns by gamma ray tomography, Chem. Eng. And Proc., 40 (2001) 209-219.

X. Ren, S. Stapf, B. Blümich, Magnetic Resonance Visualisation of Flow and Pore Structure in Packed Beds with Low Aspect Ratio, Chem. Eng. Technol., 28 (2005) 219-225.

CAPTIONS TO THE FIGURES

Figure 1: Set of images of consecutive axial cuts obtained by CT. Aspect ratio a=4.29

Figure 2: Distribution of particle centers (coordinates are normalized with tube radius)

a- Experimental data - Aspect ratio a = 5.04

b- Simulated results - Aspect ratio a = 5.04

Figure 3: Cumulative fraction of particle centers (CPC) as a function of radial coordinate ρ.

a- Experimental data - Aspect ratio a = 5.04

b- Simulated result - Aspect ratio a = 5.04

c- Simulated result - Aspect ratio a = 5.60

Figure 4: Radial distribution of particle centers (DPC) as a function of radial coordinate ρ. Aspect ratio a = 5.04. Series (♦) and (○) correspond to two slices at different axial positions of the simulated bed.

Figure 5: Comparison between experimental and predicted radial porosity profile. Aspect ratio a = 5.04. Experimental data from CT.

Figure 6: Comparison between experimental and predicted radial porosity profile. Aspect ratio a = 4.29. Experimental data from CT.

Figure 7: Comparison between experimental and predicted radial porosity profile. Aspect ratio a = 5.60. Experimental data from Benenati and Brosilow (1962)

Figure 8: Comparison between experimental and predicted radial porosity profile. Aspect ratio a = 9.30. Experimental data from Giese et al. (1998)

Figure 1

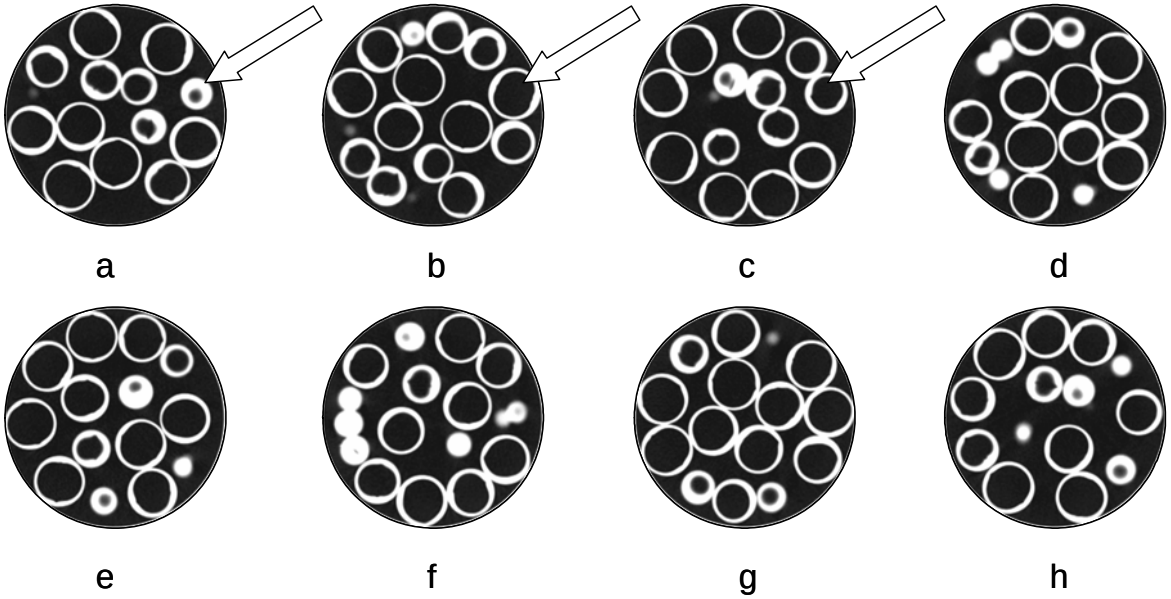

Figure 2

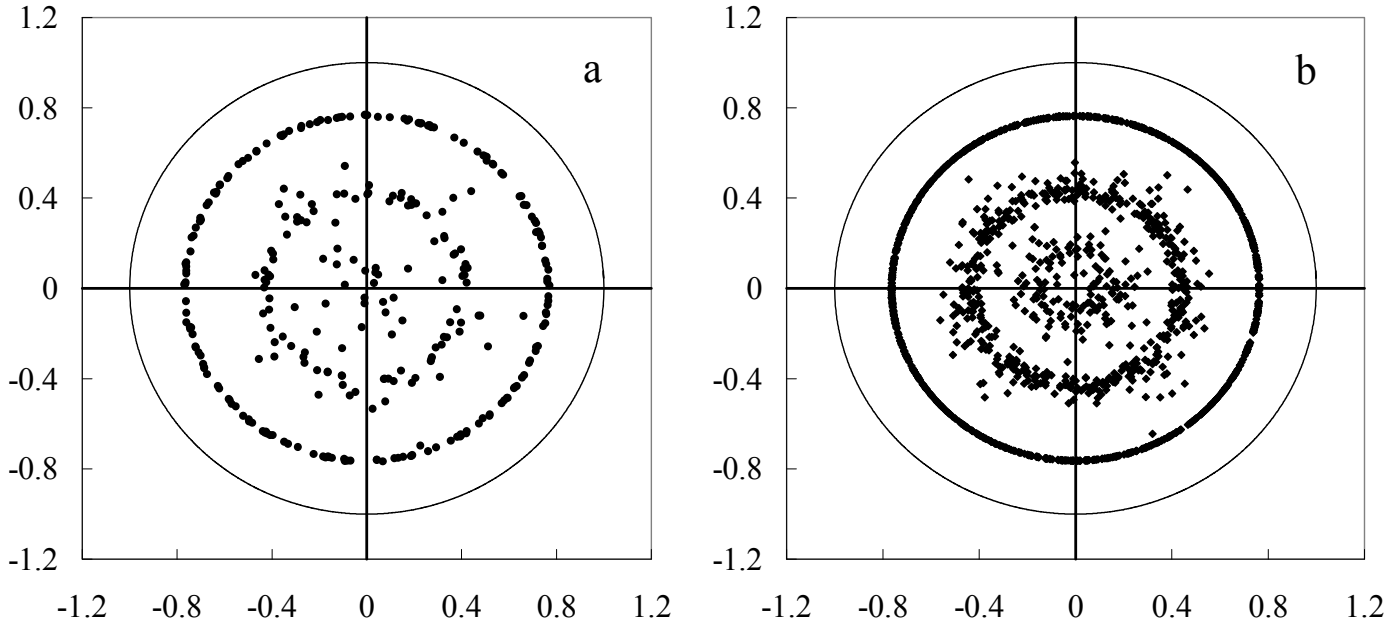

Figure 3

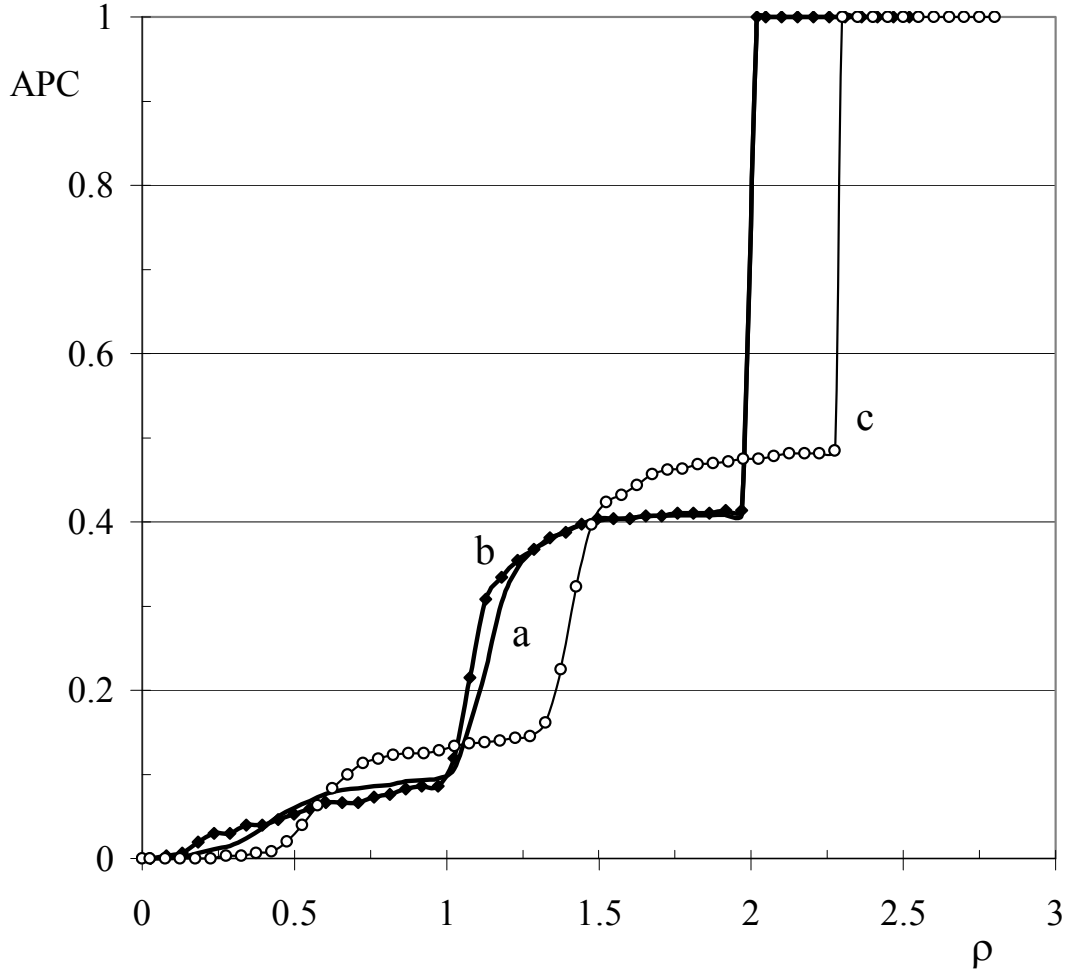

Figure 4

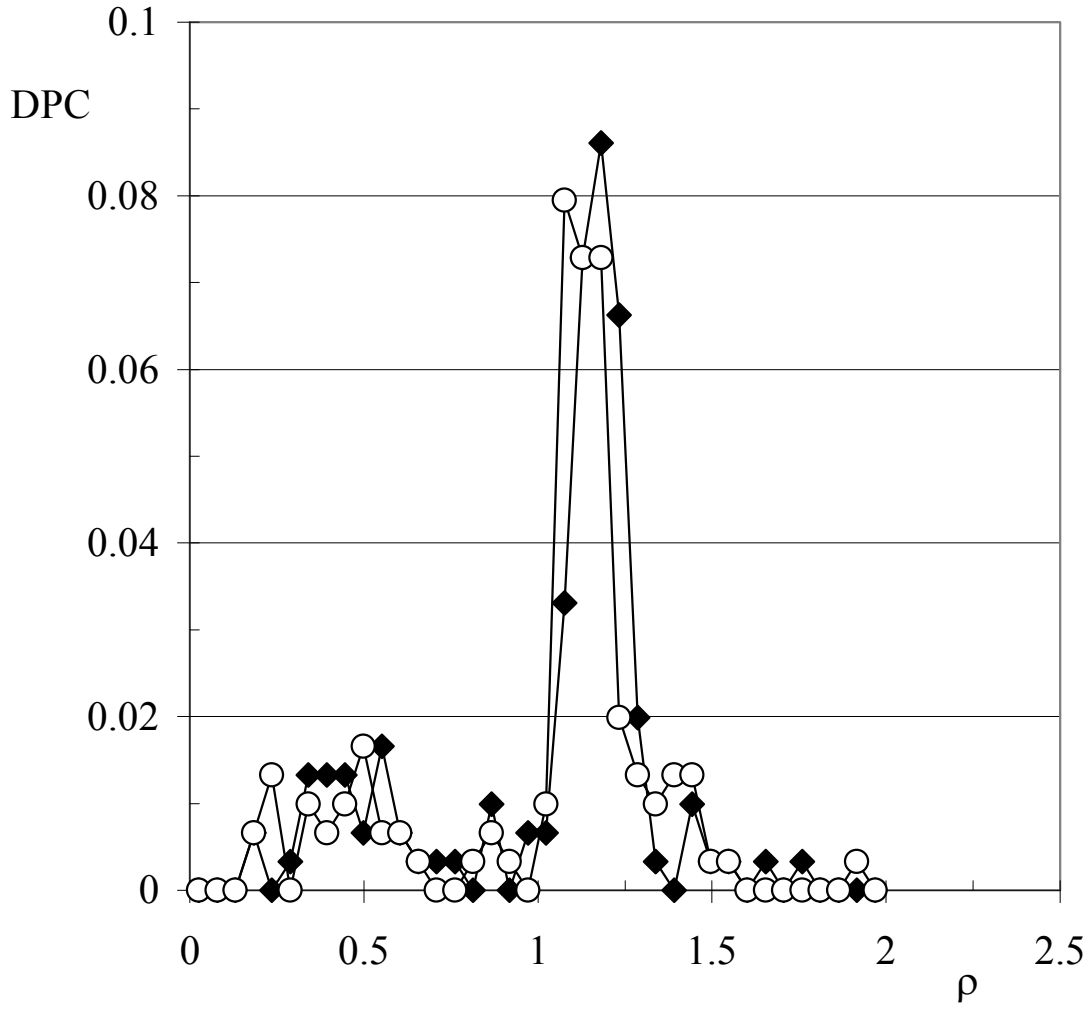

Figure 5

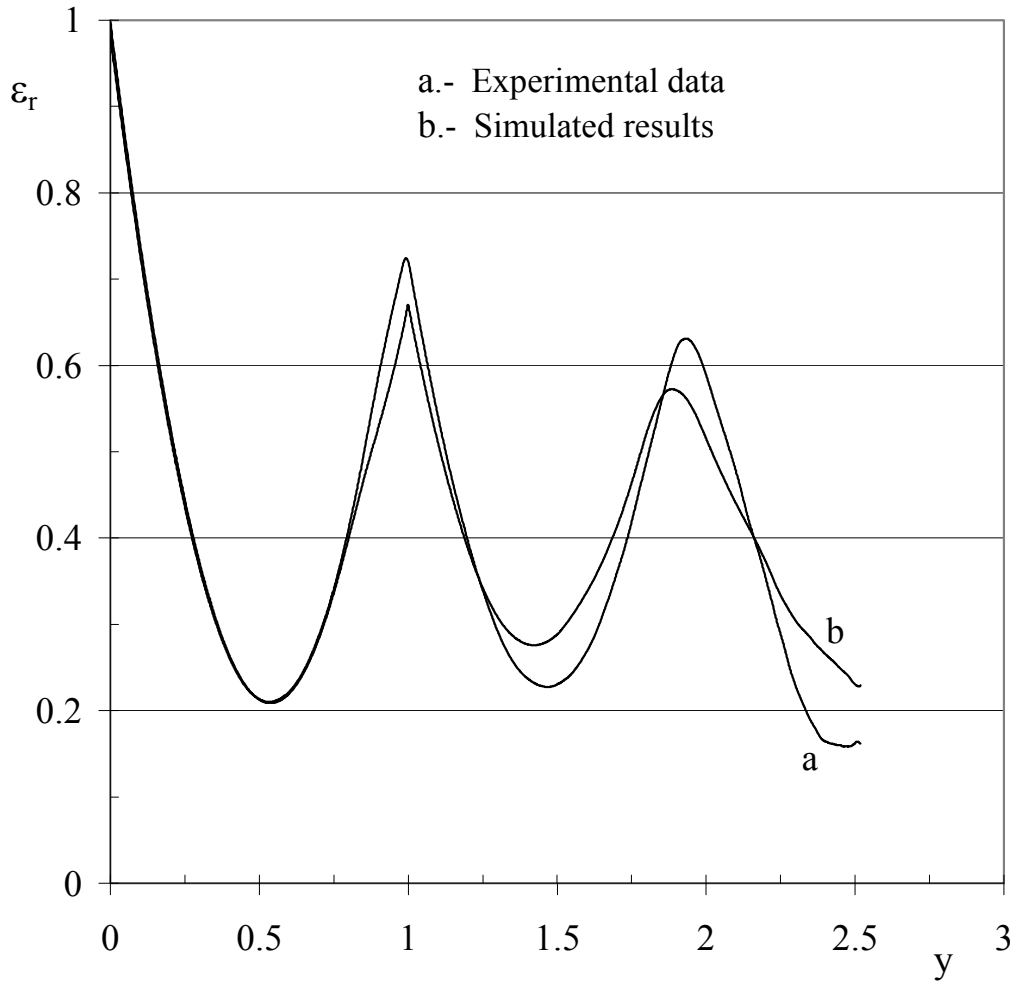
1
ε_r
a.- Experimental data
b.- Simulated results
0.8
0.6
0.4
0.2
0
b
a
0
0.5
1
1.5
2
2.5
3
y

Figure 6

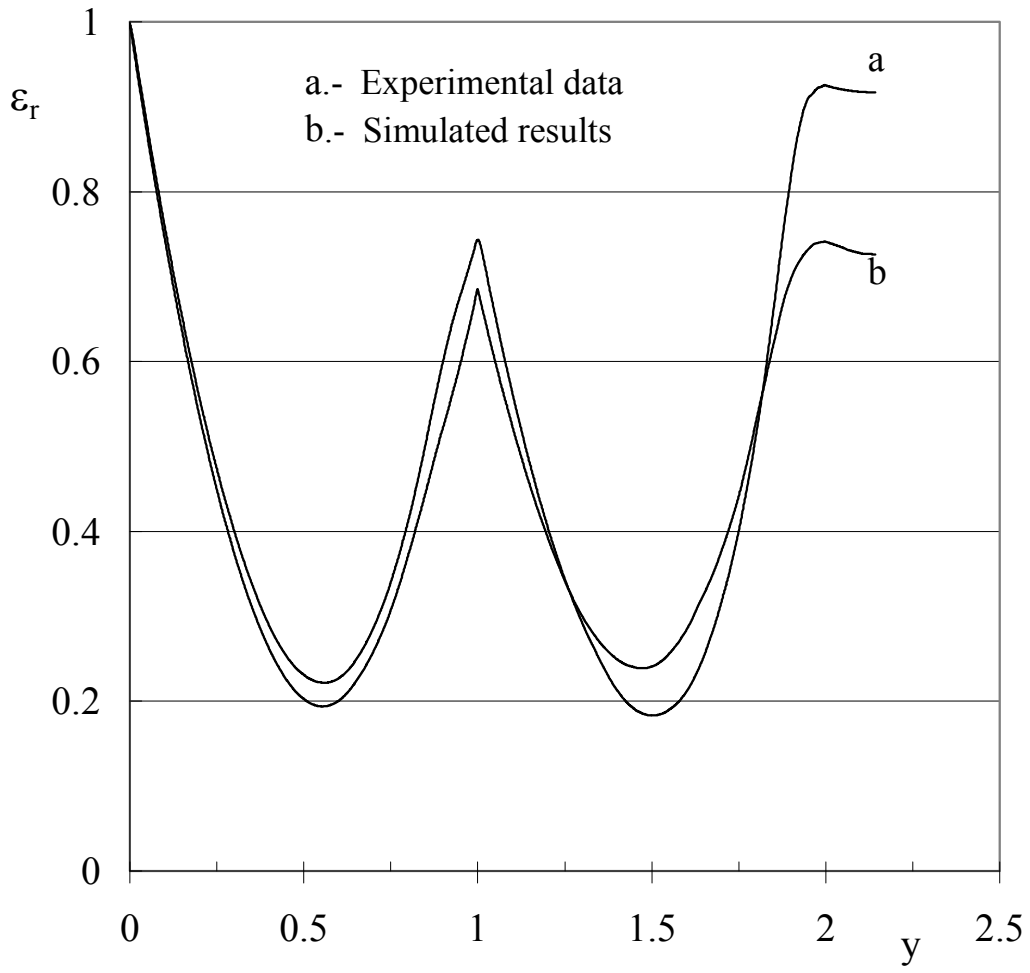
1
ε_r
a.- Experimental data
b.- Simulated results
a
b
0.8
0.6
0.4
0.2
0
0
0.5
1
1.5
2
2.5
y

Figure 7

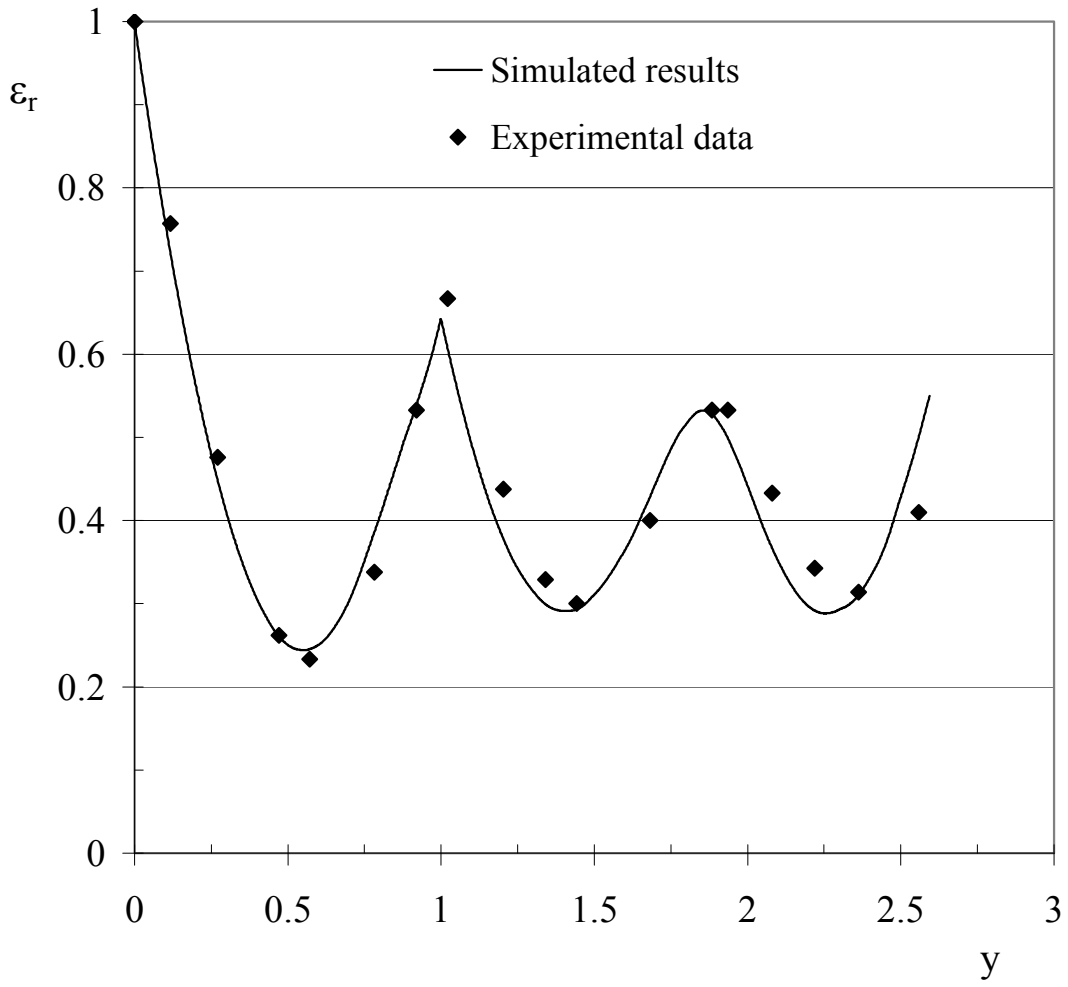
1
0.8
0.6
0.4
0.2
0
ε_r
Simulated results
Experimental data
0
0.5
1
1.5
2
2.5
3
y

Figure 8

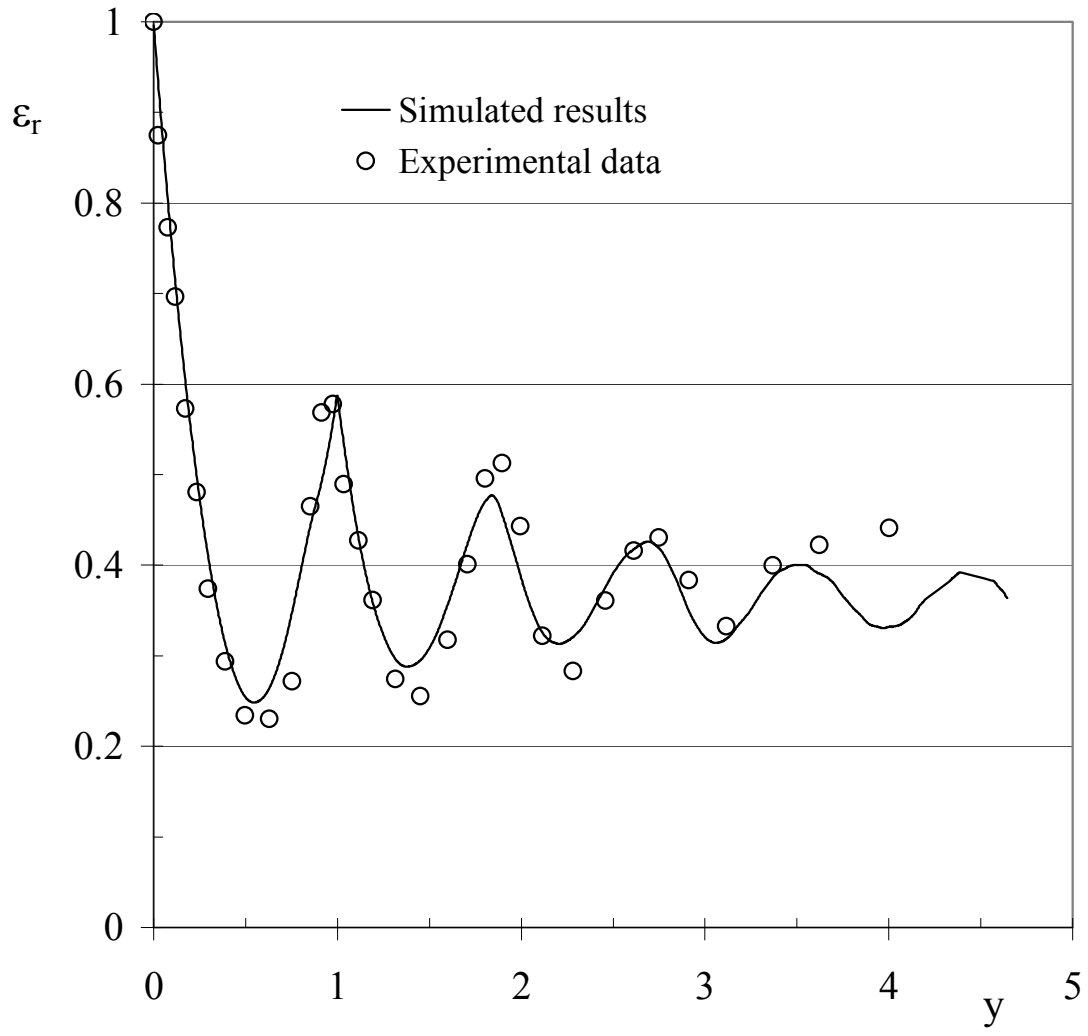
1
0.8
0.6
0.4
0.2
0
ε_r
Simulated results
Experimental data
0
1
2
3
4
5
y